

# Superconductivity on a Möbius strip: numerical studies on order parameter and quasiparticles

Masahiko Hayashi and Hiromichi Ebisawa  
Graduate School of Information Sciences, Tohoku University,  
Aramaki Aoba-ku, Sendai 980-8579, Japan  
and JST-CREST

Kazuhiro Kuboki  
Department of Physics, Kobe University, Kobe 657-8501, Japan  
(Dated: April 14, 2024)

Superconducting states of an anisotropic  $s$ -wave superconductor on a Möbius strip are studied numerically based on the Ginzburg-Landau theory and the Bogoliubov-de Gennes theory. In both, the equations are solved numerically on discretized lattice and the nonlinearity and the self-consistency are fully taken into account. First, we study the superconducting states on the Möbius strip in the presence of the Aharonov-Bohm flux threading the ring by employing the Ginzburg-Landau theory, and confirm the phase diagram previously proposed by Hayashi and Ebisawa [J. Phys. Soc. Jpn. 70, 3495 (2002)]. The metastable states as well as the equilibrium energy state are studied and the nonequilibrium processes when the magnetic field is varied at a fixed temperature are discussed. Next, we study the microscopic superconducting states on the Möbius strip based on the Bogoliubov-de Gennes theory, especially focusing on the state with a real-space node in the superconducting gap, which is expected to appear when the flux threading the ring is half the superconducting flux quantum. The local density of states in this nodal state is calculated in detail and the existence of the zero-energy bound states is shown.

PACS numbers: 74.20.De, 74.78.Na

## I. INTRODUCTION

The realization of crystals with unusual shapes, e.g., ring, cylinder etc., by Tanda et al.<sup>1,2,3</sup> has stimulated renewed interest in the effects of the system geometry on the physical properties. Especially, the synthesis of Möbius strip made of transition metal chalcogenides (NbSe<sub>3</sub>, TaS<sub>3</sub> etc.)<sup>4</sup> opens new possibility to examine the physical properties of superconductivity or charge density wave in topologically nontrivial spaces.

Recently several groups have studied physical systems on Möbius strips. Hayashi and Ebisawa<sup>5</sup> studied  $s$ -wave superconducting (SC) states on a Möbius strip based on the Ginzburg-Landau (GL) theory and found that the Little-Parks oscillation, which is characteristic to the ring-shaped superconductor, is modified for the Möbius strip and a new state, which does not appear for ordinary ring, shows up when the number of the magnetic flux quanta threading the ring is close to a half odd integer. Yakubo, Avishai and Cohen<sup>6</sup> have studied the spectral properties of the metallic Möbius strip with impurities and clarified statistical characteristics of the fluctuation of the persistent current as a function of the magnetic flux threading the ring. The persistent current in a more simplified version of the Möbius strip has also been studied by Milla, Staord and Caponi<sup>7</sup>. Wakabayashi and Harigaya<sup>8</sup> have studied the Möbius strip made of a nanographite ribbon, and the effects of Möbius geometry on the edge localized states, which is peculiar to the graphite ribbon, has been clarified. A study from a more fundamental point of view can be found in the paper by

Kaneda and Okabe<sup>9</sup> where the Ising model on Möbius strip and its domain wall structures are studied.

The main result of Ref. 5 is that if the magnetic flux threading the ring is close to a half odd integer times the flux quantum  $\Phi_0 = hc/(2e)$  ( $h, c, e$  being the Planck constant, the speed of light and the electron charge, respectively), a novel SC state appears. This state has a real-space node in SC gap along the strip: namely, the gap tends to zero along the line located in the middle of the strip. Throughout this paper we call this state the "nodal state". It has been shown that the free energy of this state can be lower than that of uniformly gapped state, which is known to be the most stable state in case of the ordinary SC rings.

This paper extends the previous study in the following two points:

- In Ref. 5, we have shown that the free energy of the nodal state is lower than other likely states. However, there is no evidence that it is the most stable. Although it is difficult to examine all possible local minimum states of the nonlinear GL free energy, in this paper we try to give a more convincing evidence by resorting to a numerical method. We perform numerical minimization of the GL free energy and find as many local minimum states as possible and reexamine the phase diagram of Ref. 5. A similar method is previously employed, for example, in Refs. 10 and 11 in studying SC disks etc.
- The electronic states, which are not treated in Ref. 5, are studied in terms of the Bogoliubov-de Gennes

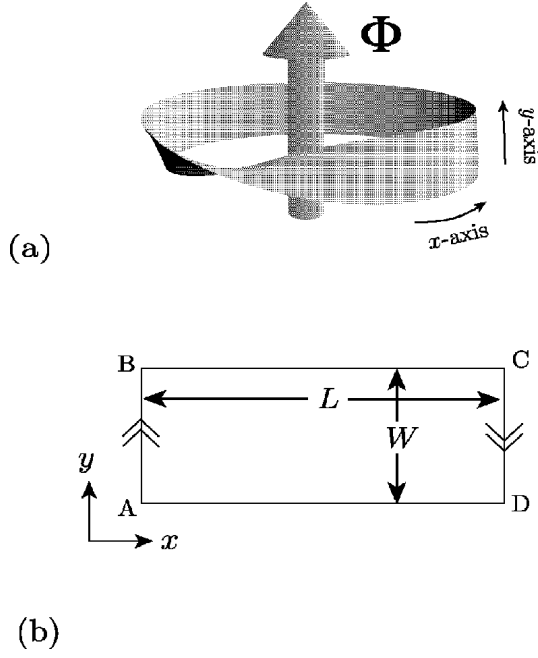


FIG. 1: (a) Geometry of SC Möbius strip where an Aharonov-Bohm flux is threading the ring (b) The developed figure of (a).

(BdG) theory. We numerically solve the BdG equation on a lattice selfconsistently, where electrons are treated by the tight-binding approximation. Based on the solution we study the local density of states in the nodal state, which may be observed, for example, by scanning tunneling microscope measurement.

This paper is organized as follows: In Sec. II, we review the behavior of a SC Möbius strip in a magnetic field, presented in Ref. 5. In Sec. III, the model, method and results of the numerical analyses of GL theory are presented. In Sec. IV, studies based on the BdG theory for the electronic properties of the nodal state are presented. In Sec. V, discussions on the results and their relation to experiments are given. Sec. VI is devoted to summary.

## II. A SUPERCONDUCTING MOBIUS STRIP IN A MAGNETIC FIELD

Here we summarize the results obtained in Ref. 5. In that paper, the behavior of a SC Möbius strip in an external magnetic field is studied based on the GL theory.

We consider the Möbius strip made of a superconductor as shown in Fig. 1 (a). The magnetic field is assumed to be threading the ring in a form of the so-called Aharonov-Bohm (AB) flux as indicated in the figure by a bold arrow, which gives rise to a non-zero vector potential on the strip although the magnetic field is vanish-

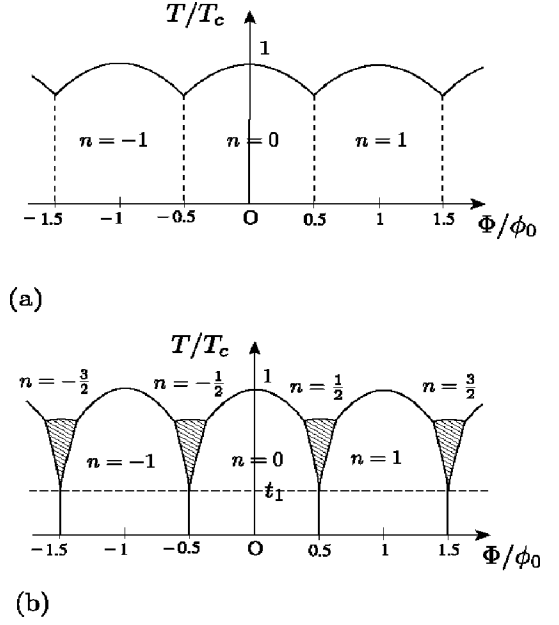


FIG. 2: Phase diagram of a superconducting Möbius strip in the presence of a AB flux with (a)  $\frac{r_k}{2} < r_?$  and (b)  $\frac{r_k}{2} > r_?$ .

ing on the strip. We further assume that the coherence length along the strip and that perpendicular to the strip, which are respectively denoted as  $\xi_k$  and  $\xi_?$ , are different. Throughout this paper we set x-axis and y-axis as indicated in the figure. The developed figure of the Möbius strip is given in Fig. 1 (b). We denote the circumference and the width by  $L$  and  $W$ , respectively.

In this paper the effects of the bending, or the non-zero curvature, caused in the strip by the Möbius geometry, are neglected. Although these may be important in the case of unconventional pairing, such as p-wave superconductors<sup>12</sup>, they may be neglected for s-wave superconductors, treated in this paper.

The equilibrium states of SC Möbius strip depends on the magnetic flux threading the ring. The SC Möbius strip shows the so-called Little-Parks oscillation of the transition temperature with a period  $\phi_0$ , as we naively expect from the analogy to the ordinary rings. However, it turned out that the oscillation can be appreciably modified in SC Möbius strip depending on the strength of the anisotropy of the coherence lengths.

The analysis of Ref. 5 shows that there are two important parameters, which are given by

$$r_? = \frac{\xi_?(0)}{W}; \quad r_k = \frac{\xi_k(0)}{L}; \quad (1)$$

where  $\xi_?(0)$  and  $\xi_k(0)$  are the coherence lengths at absolute zero temperature ( $T = 0$ ).

It has been shown that when the condition  $\frac{r_k}{2} < r_?$  is satisfied, the phase diagram in a magnetic field behaves like the one shown in Fig. 2 (a), which is basically the

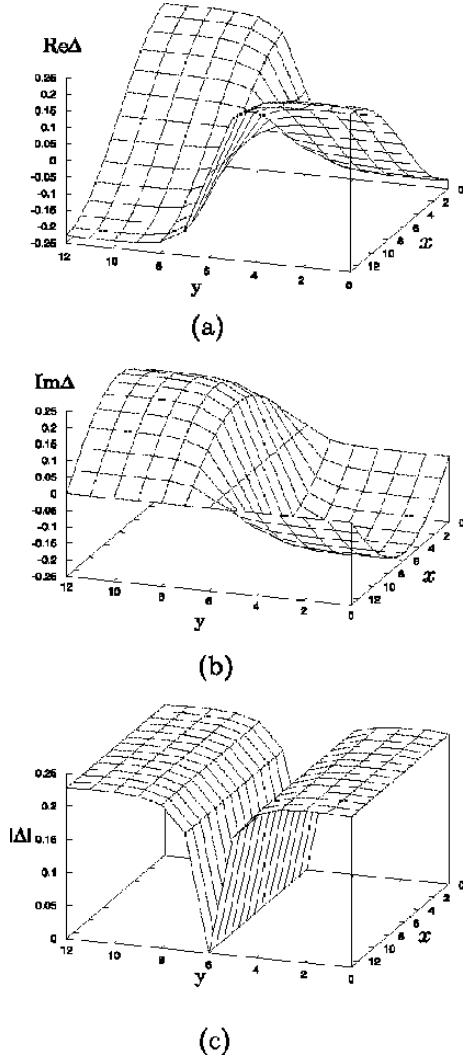


FIG. 3: (a) Real part, (b) imaginary part and (c) amplitude of the order parameter in the nodal state.

same as in the case of ordinary ring. Here  $T_c$  is the transition temperature in the bulk and the index  $n$  indicated in the figure denotes the the winding number of the phase as we go around the ring once along a trajectory parallel to the edge. When

$$\frac{\Phi_0}{2} = r_k > r_0 \quad (2)$$

is satisfied, a state characteristic to the Mobius geometry appears when the number of the flux is close to a half odd integer, as shown in Fig. 2 (b) by hatched regions. These states are indexed with a half odd  $n$  and the phase of the order parameter changes by an odd number times as we go around ring once. The spatial dependence of the order parameter is shown in Fig. 3, where the real part, the imaginary part and the amplitude are shown for  $n = 1/2$  case. It is clear that the order parameter has a real-space node in the middle of the strip. Therefore

we call these states the "nodal states". The nodal states can exist above  $t_1$  shown in Fig. 2 (b). Here  $t_1$  is given by

$$t_1 = 1 - \frac{3}{4} \frac{r_k^2}{r_0^2} \quad (3)$$

as one can see from the results in Ref. 5.

The results of Ref. 5 are obtained by comparing the free energies of the several possible states, which are chosen empirically. Therefore it is not easy to say that there is no states with lower free energies. Of course, it is impossible to investigate all possible order parameter configurations. However more reliable analysis, which can cover wider range of the configuration space is required. In this paper, to fulfill this requirement, we perform numerical study on GL theory, which is given in Sec. III.

The analysis of Ref. 5 is limited to the phenomenological one. Since the nodal state is also interesting from electronic points of view, more microscopic study is required. We solve BdG equations on the Mobius strip numerically and clarify the electronic bound state near the node of the nodal state. This will be given in Sec. IV.

### III. NUMERICAL STUDY BASED ON GINZBURG-LANDAU THEORY

In this section, we study the SC state on the Mobius strip numerically using the GL theory. Here we employ non-linear optimization method (quasi-Newton method) to find the local minimum state of the GL free energy<sup>13</sup>.

GL free energy  $F$  of our system is given as follows:

$$F = \int d^2x \left[ \frac{\hbar^2}{2m} |\nabla \psi|^2 + \frac{e}{2} \left( \frac{\partial \psi}{\partial x} \right)^2 + \frac{e}{2} \left( \frac{\partial \psi}{\partial y} \right)^2 + \frac{1}{2} \left( \frac{\partial \psi}{\partial x} \right)^2 + \frac{1}{2} \left( \frac{\partial \psi}{\partial y} \right)^2 + \frac{1}{2} \left( \frac{\partial \psi}{\partial x} \right)^2 + \frac{1}{2} \left( \frac{\partial \psi}{\partial y} \right)^2 \right] \quad (4)$$

Here  $m$ ,  $\hbar = hc/(2e)$  are the mass of a Cooper pair (twice the electron mass) and the magnetic flux quantum, respectively. The thickness of the strip  $d$  is much smaller than the superconducting coherence length and the strip can be treated as two-dimensional.  $\psi(\mathbf{r})$  and  $\mathbf{A}(\mathbf{r})$  are the SC order parameter and the vector potential, respectively.  $t = T/T_c$  is the reduced temperature. The AB flux is incorporated by taking  $\mathbf{A} = \Phi_0 \mathbf{e}_x$ , where  $\mathbf{e}_x$  is the unit vector in  $x$ -direction.  $\Phi_0$  and  $\gamma$  are positive constants, and  $\gamma = \gamma_k$  is the anisotropy parameter.

For numerical calculations we introduce the lattice ver-

sion of  $F$  as

$$\begin{aligned}
 F = F_0 & \sum_{j=1}^{N_x} \sum_{k=1}^{N_y} \tilde{\psi}(j;k) \tilde{\psi}^*(j;k) + \sum_{j=1}^{N_x} \sum_{k=1}^{N_y} \tilde{\psi}(j;k) \tilde{\psi}^*(j+1;k) \\
 & + \sum_{j=1}^{N_x} \sum_{k=1}^{N_y} \tilde{\psi}(j;k) \tilde{\psi}^*(j;k+1) + \sum_{j=1}^{N_x} \sum_{k=1}^{N_y} \tilde{\psi}(j;k) \tilde{\psi}^*(j;k+1) \\
 & + \sum_{j=1}^{N_x} \sum_{k=1}^{N_y} \tilde{\psi}(j;k) \tilde{\psi}^*(j;k+1) + \sum_{j=1}^{N_x} \sum_{k=1}^{N_y} \tilde{\psi}(j;k) \tilde{\psi}^*(j;k+1) ; \quad (5)
 \end{aligned}$$

where  $\tilde{\psi}_k = \frac{1}{\sqrt{N_x N_y}} \sum_{j=1}^{N_x} \sum_{k=1}^{N_y} \tilde{\psi}(j;k) e^{i \mathbf{a}_k \cdot \mathbf{r}_j}$ ,  $\tilde{\psi}$  is given by  $\tilde{\psi}_k(0) = d$ , where  $\tilde{\psi}_k(0) = \frac{1}{\sqrt{N_x N_y}} \sum_{j=1}^{N_x} \sum_{k=1}^{N_y} \tilde{\psi}(j;k) e^{i \mathbf{a}_k \cdot \mathbf{r}_j}$  and  $d$  is the lattice spacing. Here the lattice is assumed to be a square one. Note that  $N_x d = L$  and  $N_y d = W$ .  $F_0$  is  $V_0^{-2}$  where  $V_0 = d^2 \epsilon_0$ . The order parameter  $\tilde{\psi}$  is normalized so that  $|\tilde{\psi}| \leq 1$  as  $t \rightarrow 0$ .

We use the open boundary condition in  $y$ -direction and periodic boundary condition in  $x$ -direction: namely, we put

$$\tilde{\psi}(N_x + 1; k) = \tilde{\psi}(1; N_y + 1 - k); \quad (6)$$

$(1 - k - N_y)$  in the first two lines of Eq. (5).

The order parameter  $\tilde{\psi}(j;k)$  minimizing  $F$  is obtained by solving the equation,

$$\frac{\partial F}{\partial \tilde{\psi}(j;k)} = 0; \quad (7)$$

which yields,

$$\begin{aligned}
 & \tilde{\psi}(j+1;k) e^{i \mathbf{a}_k \cdot \mathbf{r}_{j+1}} + \tilde{\psi}(j-1;k) e^{i \mathbf{a}_k \cdot \mathbf{r}_{j-1}} \\
 & + 2 \tilde{\psi}(j;k+1) + 2 \tilde{\psi}(j;k-1) + 2(1 - t) \tilde{\psi}(j;k) \\
 & + (t - 1) \tilde{\psi}(j;k) + \tilde{\psi}(j;k) \tilde{\psi}^*(j;k) \tilde{\psi}(j;k) = 0; \quad (8)
 \end{aligned}$$

We obtained the solution of the Eq. (8) in terms of the nonlinear optimization of the free energy Eq. (5). In this paper we especially utilized the so-called quasi-Newton method<sup>13</sup>. Like other methods of nonlinear optimization, quasi-Newton method starts from an initial value of  $\tilde{\psi}$  and changes it so that the free energy becomes lower until finally we reach the local minimum. Therefore which local minimum we reach depends on the initial value of  $\tilde{\psi}$ . In this paper we randomly chose the initial values and performed optimization as many times as possible. Then we obtained several local minimum states. These procedure is the same as the one adopted in Refs. 10 and 11.

The results are as follows. The system size we used is  $N_x = 10, N_y = 10, \phi_0 = 1.5d$  and  $\epsilon = 1.2d$ .

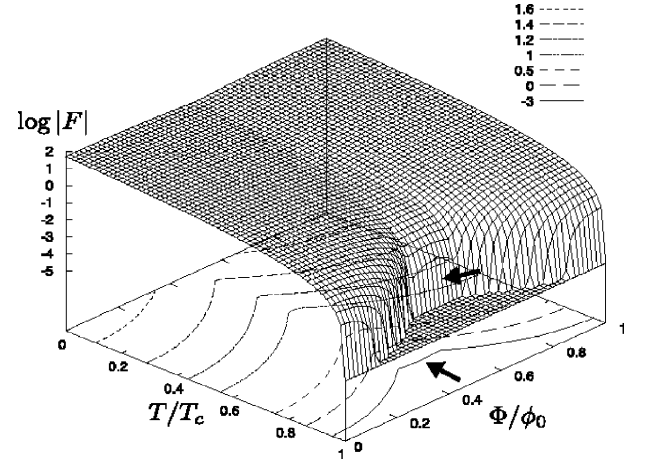


FIG. 4: The free energy of the most stable state as a function of  $T$  and  $\Phi$ . Around  $\Phi/\phi_0 = 2$  a structure corresponding to the nodal state can be seen. The vertical axis is the logarithm of the  $F$  and the region with  $F < 10^{-5}$  near  $T_c$  has been cut off. The free energy is measured in the unit of  $F_0$ .

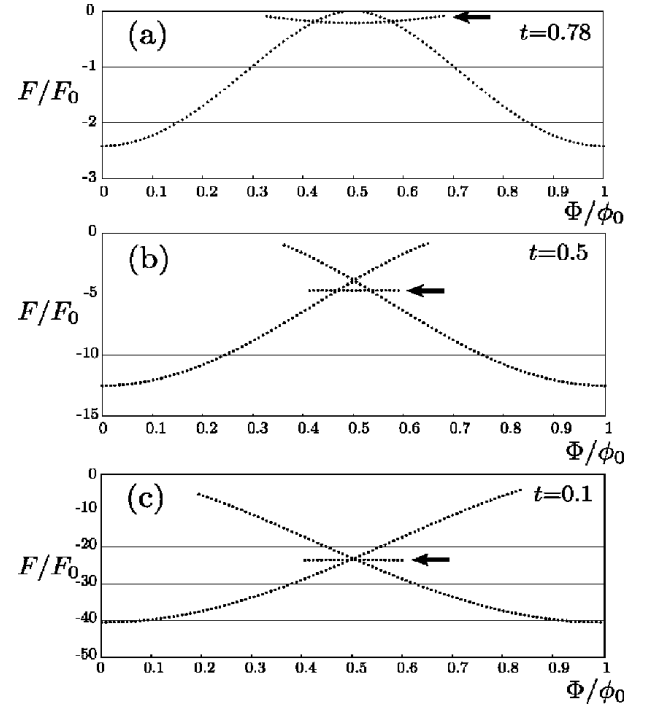


FIG. 5: The free energy of the metastable states as a function of  $\Phi$  for (a)  $t = 0.78$ , (b)  $t = 0.5$ , and (c)  $t = 0.1$ . The branches corresponding to the nodal states are indicated by bold arrows in every graph. It becomes the most stable state when  $t = 0.78$  and  $0.5$  for a certain region of  $\Phi$ . When  $t = 0.1$  there is no stable region for the nodal state.

First we discuss the phase diagram. The numerically obtained free energy is shown in Fig. 4 using the log scale: we have shown only the region with  $F < 0$  and  $\log F_j$  is plotted as a function of  $\phi$  and  $T$ . We can see from this figure that the structure corresponding to the nodal state appears near  $\phi = 0=2$  (shown by bold arrows). Actually, the order parameter in this region behaves like that shown in Fig. 3.

In Fig. 5, we have depicted the free energies of the metastable states at three different temperatures (a)  $t = 0.78$ , (b)  $t = 0.5$  and (c)  $t = 0.1$ . We clearly see three distinct series of states in each graph. The branch which starts from  $\phi = 0$  corresponds to the state with a uniform order parameter  $\phi = (\text{const.})$  and that ends at  $\phi = 0$  corresponds to the state with  $\phi = (\text{const.}) e^{i2\pi x/L}$ . Between these two branches, a branch corresponding to the nodal state can be seen. At  $t = 0.78$  and  $t = 0.5$ , the nodal state has the lowest free energy near  $\phi = 0=2$ . However, at  $t = 0.1$ , although the nodal state is still a metastable state, there is no region where the nodal state is the most stable. These features agree with the prediction of Ref. 5.

#### IV. NUMERICAL STUDY BASED ON BOGOLIUBOV-DE GENNES THEORY

In order to study the s-wave SC state on a Mobius strip microscopically, we treat a tight-binding model on a square lattice with attractive on-site interactions. The Hamiltonian of the system is given as

$$H = \sum_{\mathbf{j}} t_x (e^{i\phi} c_{\mathbf{j}+\hat{x}}^\dagger c_{\mathbf{j}} + e^{-i\phi} c_{\mathbf{j}}^\dagger c_{\mathbf{j}+\hat{x}}) + \sum_{\mathbf{j}} t_y (c_{\mathbf{j}+\hat{y}}^\dagger c_{\mathbf{j}} + c_{\mathbf{j}}^\dagger c_{\mathbf{j}+\hat{y}}) + \sum_{\mathbf{j}} V n_{\mathbf{j}\uparrow} n_{\mathbf{j}\downarrow} \quad (9)$$

where  $c_{\mathbf{j}}$  is the annihilation operator of electron at a site  $\mathbf{j}$  with spin ( $\uparrow, \downarrow$ ), and  $V (> 0)$  and  $\phi$  are the attractive interaction and the chemical potential, respectively. Here  $\mathbf{j} = (j_x, j_y)$  ( $1 \leq j_x \leq N_x, 1 \leq j_y \leq N_y$ ) numbers the sites, where  $N_x$  and  $N_y$  are the numbers of sites along the x- and y-direction, respectively, and  $\hat{x} = (1; 0)$ ,  $\hat{y} = (0; 1)$ .  $n_{\mathbf{j}} = c_{\mathbf{j}}^\dagger c_{\mathbf{j}}$  is the electron number operator. The transfer integrals for x- and y-directions are denoted as  $t_x$  and  $t_y$ , respectively, and the Peierls phase  $\phi = (\hbar/2m_x)(\hbar/2m_y)$  represents the effect of the AB flux threading the Mobius strip. To realize the Mobius geometry we impose, for x-direction, the condition,

$$c_{(N_x+1; j_y)} = c_{(1; N_y - j_y + 1)}; \quad (10)$$

while for the y-direction we assume the open boundary condition.

The interaction term is decoupled within a mean-field approximation as

$$n_{\mathbf{j}\uparrow} n_{\mathbf{j}\downarrow} \approx \langle n_{\mathbf{j}\uparrow} \rangle n_{\mathbf{j}\downarrow} + \langle n_{\mathbf{j}\downarrow} \rangle n_{\mathbf{j}\uparrow} - \langle n_{\mathbf{j}\uparrow} \rangle \langle n_{\mathbf{j}\downarrow} \rangle \quad (11)$$

with  $\langle n_{\mathbf{j}\uparrow} \rangle \langle n_{\mathbf{j}\downarrow} \rangle$  being the SC order parameter. Then the mean-field Hamiltonian is written as

$$H_{\text{MFA}} = \sum_{\mathbf{j}, \mathbf{k}} \begin{pmatrix} c_{\mathbf{j}} & c_{\mathbf{j}+\hat{x}} \end{pmatrix} \begin{pmatrix} W_{\mathbf{j}\mathbf{k}} & F_{\mathbf{j}\mathbf{k}} \\ F_{\mathbf{j}\mathbf{k}}^* & W_{\mathbf{j}\mathbf{k}} \end{pmatrix} \begin{pmatrix} c_{\mathbf{k}} \\ c_{\mathbf{k}+\hat{x}} \end{pmatrix} \quad (12)$$

where

$$h_{\mathbf{j}\mathbf{k}} = \begin{pmatrix} W_{\mathbf{j}\mathbf{k}} & F_{\mathbf{j}\mathbf{k}} \\ F_{\mathbf{j}\mathbf{k}}^* & W_{\mathbf{j}\mathbf{k}} \end{pmatrix}; \quad \mathbf{j}, \mathbf{k} \quad (13)$$

with

$$\begin{aligned} W_{\mathbf{j}\mathbf{k}} &= t_x (e^{i\phi} c_{\mathbf{k}+\hat{x}}^\dagger c_{\mathbf{j}} + e^{-i\phi} c_{\mathbf{j}}^\dagger c_{\mathbf{k}+\hat{x}}) \\ F_{\mathbf{j}\mathbf{k}} &= t_y (c_{\mathbf{k}+\hat{y}}^\dagger c_{\mathbf{j}} + c_{\mathbf{j}}^\dagger c_{\mathbf{k}+\hat{y}}) \end{aligned} \quad (14)$$

By solving the following BdG equation

$$\sum_{\mathbf{l}} h_{\mathbf{j}\mathbf{l}} \begin{pmatrix} u_{\mathbf{l}n} \\ v_{\mathbf{l}n} \end{pmatrix} = E_n \begin{pmatrix} u_{\mathbf{j}n} \\ v_{\mathbf{j}n} \end{pmatrix} \quad (15)$$

we can obtain the energy eigenvalues  $E_n$  and the corresponding eigenfunctions  $(u_{\mathbf{j}n}; v_{\mathbf{j}n})$ , where  $n$  is numbering the states. The unitary transformation using  $(u_{\mathbf{j}n}; v_{\mathbf{j}n})$  diagonalizes  $H_{\text{MFA}}$ , and the SC order parameter  $\phi$  can be written in terms of  $E_n$  and  $(u_{\mathbf{j}n}; v_{\mathbf{j}n})$ . These constitute the self-consistency equations which will be solved numerically. In the following we take the parameters as,

$$\begin{aligned} t_x &= 1.0; \quad t_y = 0.49 \\ \phi &= 0; \quad T = 0.22; \quad V = 0.25; \end{aligned} \quad (16)$$

First we estimate the correlation lengths,  $\xi_x(0)$  and  $\xi_y(0)$ , by calculating the anomalous Green's function  $F(\mathbf{j}) = \langle c_{\mathbf{k}\uparrow} c_{\mathbf{k}+\mathbf{j}\uparrow} \rangle$  at  $T = 0$  without applying the magnetic flux, and the results are depicted in Fig. 6. (This calculation has been carried out in a larger system with  $100 \times 100$  sites using periodic boundary condition for both x- and y-directions.) From the results in Fig. 6 and the relation  $F(\mathbf{j}) / \exp(-|\mathbf{j}|d)$ ,  $\xi_x(0)$  and  $\xi_y(0)$  are estimated as

$$\xi_x(0) = 2.37d; \quad \xi_y(0) = 0.64d; \quad (17)$$

where  $d$  is the lattice spacing.

The calculation in the Mobius geometry is carried out for a system with  $N_x = 13$  and  $N_y = 14$ . Putting  $L = 13d$  and  $W = 14d$ , we obtain  $r_x = 0.18$  and  $r_y = 0.046$ . These values satisfy the condition, Eq. (2). Furthermore,  $t_1$  is estimated to be  $13$ , which means that the nodal state is stable at all temperature range down to  $0K$ . In passing, the bulk  $T_c$  of this system is  $0.358$  (estimated numerically in the system with  $100 \times 100$  sites), which coincides with that in  $13 \times 14$  system with  $\phi = 0$  within a numerical accuracy.

In this calculation, we limited ourselves to the case of the nodal state at  $\phi = 0=2$ . Since this microscopic calculation needs more time to obtain good convergence as compared to GL calculation, we have selected for the

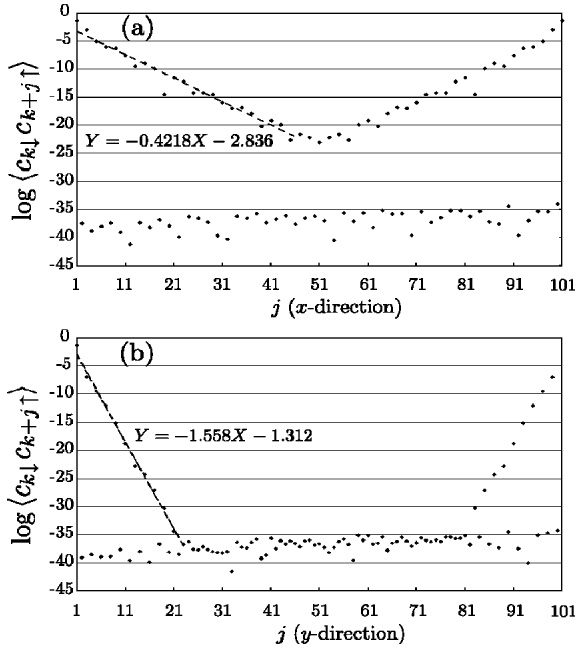


FIG. 6: The anomalous correlation function  $\log \langle C_{k\downarrow} C_{k+j\uparrow} \rangle$  for the system with the parameters in Eq. (16). (a) and (b) correspond to the correlation in the x- and y-direction, respectively. The equations in the figures are the approximating lines to the exponential decay.

initial order parameter the solution obtained by the GL analysis, such as the one depicted in Fig. 3. After the calculation, the behavior of the order parameter has not changed so much and we consider that the iteration converged to the nodal state. The local density of states (LDOS) is calculated from the equation,

$$N(j; E) = \frac{1}{-\text{Im}} \sum_n \frac{u_{jn} u_{jn}}{E - E_n + i} : \quad (18)$$

where  $\gamma$  is the broadening of the single energy level, introduced to simulate the actual experiment. The result is shown in Fig. 7 with  $\gamma = 0.03$ . Each line of Fig. 7 corresponds to the LDOS at  $j = (1; j_y)$  where  $j_y$  numbers the chain from the edge of the strip. (The LDOS is independent of  $j_x$ .) Because of the inversion symmetry with respect to the center, we depicted LDOS only for  $1 \leq j_y \leq 7$ , where  $j_y = 1$  and  $j_y = 7$  correspond to the outermost and the innermost chain, respectively.

In Fig. 7, a well-developed gap behavior can be seen for  $1 \leq j_y \leq 5$  and the bound states are formed in the chains  $j_y = 6$  and 7. These bound states originate from the node. Since the node can be regarded as the spontaneously formed  $\pi$ -junction (as one can see from Fig. 3, the phase of the order parameter changes by  $\pi$  in crossing the node), the bound state energy must be zero. In Fig. 7, the deviation from zero energy is seen, which may be due to the finite size effect. This point will be discussed in detail in a separate paper<sup>14</sup>.

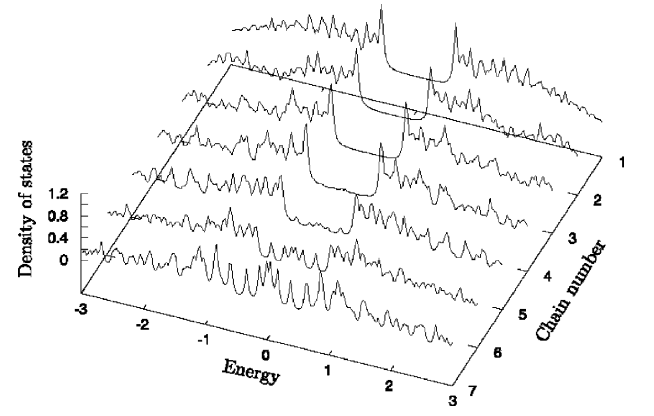


FIG. 7: The local density of state in the nodal state on the M obius strip

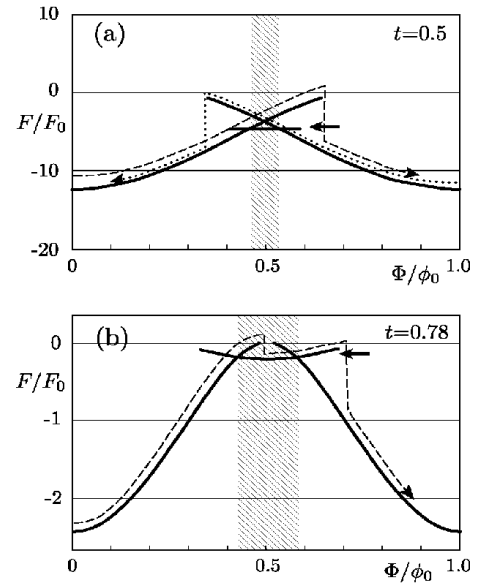


FIG. 8: The transition of the states in the field sweep experiment for (a)  $t = 0.5$  and (b)  $t = 0.78$ . The nodal state is the most stable in the shaded region. See text for the details.

## V. DISCUSSION

In this paper, by using the numerical methods, we have confirmed that the predictions of Ref. 5 are satisfied within both GL and BdG level. Until now, we have limited our discussion to purely two-dimensional cases. This is not the case for actually synthesized M obius crystals<sup>4</sup>. Here we discuss the effects of the finite thickness of the strip. If the M obius strip is thicker than the SC coherence length perpendicular to the strip surface, the nodal

state may no longer be stable and the node, which is obtained under the assumption that the gap is uniform in the direction of the thickness, may become a vortex line, embedded inside the strip. Then there is no gapless region on the surface. In this case, we can not observe the node by only measuring the surface density of states by scanning tunneling microscope. The observation of the nodal state may be possible only by measuring the variation of the gap or magnetization as a function of the magnetic flux. More precise analysis on the thicker MoBiS strips is left for the future study.

In Sec. III, we have calculated the free energies not only of the equilibrium state but also of the metastable states. The metastable states do not appear in the thermodynamic equilibrium, though they play important roles in actual experiments in which one sweeps the magnetic flux<sup>15,16,17,18</sup>. As shown by the previous studies, when we change the magnetic flux the state of the system remains in one of the metastable states and it does not switch to another lower-energy state until the initial state finally becomes unstable. Although there may be effect of thermally assisted tunneling, such effects are limited to the very vicinity of the critical temperature. From these we point out a possibility that the nodal state may not appear at all in the field sweep experiment even though it can be a true equilibrium state for some values of the flux. This is understood from the Fig. 8 (a), where the free energy for  $t = 0.5$  and the time evolution of the system under a field sweep process are shown. The bold curves show the free energies of the metastable states and the equilibrium state at  $t = 0.5$ . The branch corresponding to the nodal state is indicated by a bold arrow. The dashed and dotted curves show the time evolution of the

system in up- and down-sweep experiment, respectively, where it is assumed that the transition between different branches are prohibited by the energy barrier except when the system comes to the end of a branch. In this case, although the nodal state can be a true equilibrium state, it does not appear during the field sweep process. In contrast to this, the nodal state appears during the field sweep process at  $t = 0.78$ , as shown in Fig. 8 (b) (Only up-sweep process is indicated). Therefore the observability of the nodal state in the field-sweep experiment may be further limited to the region in the vicinity of the critical temperature. More precise numerical simulation is required to clarify these dynamical processes of this system quantitatively, which is left for future studies.

## VI. SUMMARY

In this paper, we have investigated the superconducting states on a MoBiS strip in terms of the numerical analyses based on Ginzburg-Landau and Bogoliubov-de Gennes theory. It has been shown that in the MoBiS geometry a novel nodal state can appear both in equilibrium and metastable states. The experimental observability of the nodal states is discussed based on the findings.

Acknowledgments

M.H. and H.E. were financially supported by Grants-in-Aid for Scientific Research of Ministry of Education, Science, and Culture. K.K. was financially supported by the Sumitomo Foundation.

---

Electronic address: hayashi@cm.t.tohoku.ac.jp

<sup>1</sup> S. Tanda, H. Kawamoto, M. Shiobara, Y. Okajima, and K. Yamaya, J. Phys. IV France 9, 379 (1999).

<sup>2</sup> S. Tanda, H. Kawamoto, M. Shiobara, Y. Sakai, S. Yasuzuka, Y. Okajima, and K. Yamaya, Physica B 284-288, 1657 (2000).

<sup>3</sup> Y. Okajima, H. Kawamoto, M. Shiobara, K. Matsuda, S. Tanda, and K. Yamaya, Physica B 284-288, 1659 (2000).

<sup>4</sup> S. Tanda, T. Tsuneta, Y. Okajima, K. Inagaki, K. Yamaya, and N. Hatakenaka, Nature 417, 397 (2002).

<sup>5</sup> M. Hayashi and H. Ebisawa, J. Phys. Soc. Jpn. 70, 3495 (2002).

<sup>6</sup> K. Yakubo, Y. Avishai, and D. Cohen, Phys. Rev. B 67, 125319 (2003).

<sup>7</sup> F. Milla, C. Staud, and S. Capponi, Phys. Rev. B 57, 1457 (1998).

<sup>8</sup> K. Wakabayashi and K. Harigaya, J. Phys. Soc. Jpn. 72, 998 (2003).

<sup>9</sup> K. Kaneda and Y. Okabe, Phys. Rev. Lett. 86, 2134

(2001).

<sup>10</sup> V. A. Schweigert, F. M. Peeters, and P. S. Deo, Phys. Rev. Lett. 81, 2783 (1998).

<sup>11</sup> B. J. Baelus, F. M. Peeters, and V. A. Schweigert, Phys. Rev. B 61, 9734 (2000).

<sup>12</sup> M. Sigrist and K. Ueda, Rev. Mod. Phys. 63, 239 (1991).

<sup>13</sup> W. H. Press, B. P. Flannery, S. A. Teukolsky, and W. T. Vetterling, Numerical Recipes in C (Cambridge University Press, 1988).

<sup>14</sup> T. Suzuki, M. Hayashi, H. Ebisawa, and K. Kuboki, in preparation.

<sup>15</sup> B. J. Baelus, F. M. Peeters, and V. A. Schweigert, Phys. Rev. B 63, 144517 (2001).

<sup>16</sup> V. A. Schweigert and F. M. Peeters, Phys. Rev. Lett. 83, 2409 (1999).

<sup>17</sup> A. Kanda and Y. Otuka, Physica B 329-333, 1421 (2003).

<sup>18</sup> A. Kanda and Y. Otuka, Physica C 404, 205 (2004).